Imperfect Fabry-Perot resonators

Klaassen, T.

CHAPTER 5

Gouy phase of nonparaxial eigenmodes in a folded resonator

We study the effect of nonparaxiality in a folded resonator by accurate measurements of the Gouy phase, as function of the mode number for mode numbers up to 1500*. Our experimental method is based upon tuning the resonator close to a frequency-degenerate point. The Gouy phase shows a nonparaxial behavior that is much stronger in the folding-plane than in the perpendicular plane. Agreement with ray-tracing simulations is established and a link with aberration theory is made.*

T. Klaassen, A. Hoogeboom, M. P. van Exter, and J. P. Woerdman, J. Opt. Soc. Am. A **21***, 1689-1693 (2004).*

5.1 Introduction

Our interest is in the spectrum of a folded (3-mirror) optical resonator; this is stimulated by the fact that Dingjan *et al.* [55] have recently found a signature of wave chaos in such a resonator. Generally, to obtain wave chaos, a minimum requirement is that the wave equation describing the system is nonseparable. This can be achieved by making the numerical aperture of the resonator relatively large, *i.e.*, going beyond the paraxial regime. Since in this regime aberrations occur, it is natural to look for a connection between the basic concept of a paraxial resonator, namely its Gouy phase, and optical aberration theory. In the present Chapter, we make this connection by extending the concept of the Gouy phase, which is essentially a paraxial concept, into the nonparaxial domain where optical aberrations form the more natural concept. Our approach is mainly experimental; it is based on accurate measurements of the Gouy phase, being the diffraction-induced phase delay of a finite-diameter focused beam as compared to a plane wave. By measuring this phase difference for transverse modes up to very high mode numbers (beyond paraxiality), we can obtain quantitative information on the optical aberrations in the cavity. In principle, a connection with standard lens aberration theory can be made by realizing that the optical cavity (a folded one in our case) is equivalent to a periodic lens guide [12]. However, this comparison is hampered by the fact that we deal with a highly unusual series of lenses as shown in Fig. 5.8b below (periodic; relatively large separations; strongly astigmatic elements), which does not appear in the literature on lens aberrations.

In Section 5.2, we introduce the theory of the Gouy phase. The experiment is described in Section 5.3 and the experimental results are discussed in Section 5.4. In Section 5.5, we present ray-tracing calculations and compare them with the experimental results. The results are explained using aberration theory in Section 5.6 and we summarize our work in Section 5.7.

5.2 Gouy phase theory

The Gouy phase is an essential ray- and wave-property of optical resonators [12, 21, 46]; it plays an important role in determining the position and slope of the intra-cavity rays and the spectral properties of the modes. These modes can be chosen as Hermite-Gaussian eigenmodes with eigenfrequencies

$$\nu_{q,nm} = \frac{c}{2L}\left[q + (m+n+1)\frac{\theta_0}{2\pi}\right] , \tag{5.1}$$

where θ_0 is the Gouy phase, L the length of the cavity and q, n and m are the longitudinal and transversal mode numbers, respectively. Throughout this Chapter, we choose $n = 0$ as we excite in the experiment discussed below only a set of 1-dimensional modes. The longitudinal mode spacing is called the free spectral range: $\Delta\nu_{\mathrm{FSR}} = c/2L$. Frequency-degeneracy occurs when the Gouy phase is equal to a rational fraction of 2π, $\theta_0 = 2\pi K/N$. In the ray picture, N longitudinal round-trips are then needed before the ray returns on itself [21], and K is the number of transverse "round-trips" an orbit makes before closing; in all our experiments, we use a resonator configuration that yields $K = 1$. The frequency-degenerate eigenfrequencies

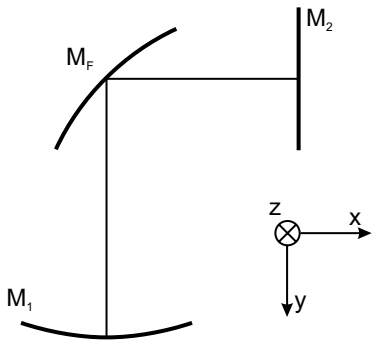

Figure 5.1: *The folded 3-mirror resonator and its orientation.*

in the spectrum are thus

$$\nu_{q,m0} = \frac{c}{2LN}\left[Nq + (m+1)\right] , \tag{5.2}$$

which implies that when we raise m by N and at the same time lower q by 1 that $\nu_{q,m}$ and $\nu_{q-1,m+N}$ are the same. The spectrum collapses into N "clumps" of modes.

For the fundamental Gaussian mode, the Gouy phase θ_0 is defined as the round-trip phase delay ψ_0 between this mode and a plane wave. Higher-order TEM_{m0} modes experience a larger phase delay ψ_m as compared to the reference plane wave; in the paraxial regime, we have simply $\psi_m \equiv (m+1)\theta_0$ [12]. In the nonparaxial regime, we can similarly define an m-dependent Gouy phase θ_m via $\theta_m = (\psi_m - \psi_0)/m$. Any m-dependence of θ_m, *i.e.*, any change in Gouy phase as a function of the mode number, is equivalent to the presence of aberrations with respect to paraxiality.

Next, we consider a folded 3-mirror resonator, with a folding angle of, *e.g.*, 90°, and a *spherical* folding mirror (Fig. 5.1); note that when using a *planar* folding mirror, the folded 3-mirror cavity is trivially equivalent with a two-mirror cavity. Already in the paraxial regime, the effective power of the folding mirror in the xz-principal plane is different from the effective power in the y-principal plane. This trivial form of astigmatism causes that *two* Gouy phases are needed to describe the resonator. The same degeneracy N requires different lengths of the resonator in the xz-principal plane and the y-principal plane.

In the nonparaxial regime, the folding mirror affects the magnitude of the aberrations in both planes of the folded resonator. The modes in the y-principal plane will hardly feel the aberrations of the folding mirror. In contrast, the modes in the xz-principal plane, will undergo the full effect of the aberrations introduced by the folding mirror; these will be stronger than in the case of a two-mirror resonator.

Since we operate close to frequency-degeneracy, the Gouy phase θ_m for an arbitrary mode m (integer multiple of N) can be written as

$$\theta_m = \frac{2\pi}{N} + \Delta\theta_m , \tag{5.3}$$

where θ_m is the Gouy phase and $\Delta\theta_m$ parametrizes how close the spectrum is to degeneracy. A generalization of Eq. 5.1, along the lines described above, using $\theta_m = (\psi_m - \psi_0)/m$, shows

that $\Delta\theta_m$ can experimentally be found from

$$\Delta\theta_m = \frac{2\pi}{\Delta\nu_{\mathrm{FSR}}}\frac{\Delta\nu_m}{m}\,, \tag{5.4}$$

where m is the transverse mode number, $\Delta\nu_m$ is the frequency difference of the fundamental mode and mode m, and $\Delta\nu_{\mathrm{FSR}}$ is the free spectral range.

5.3 Experiment

Our folded optical resonator (Fig. 5.1) consists of three highly reflective mirrors (nominal specification $R > 99.995\%$). The folding angle is 90°, the radii of curvature of mirror M_1 and M_F are 1 m, mirror M_2 is planar, and all mirrors have a diameter of 2.5 cm. Fig. 5.2 shows the complete experimental setup. The length of arm A_2 is 1.2 cm, the length of arm A_1 is variable. We probe the transmission of the resonator with a beam at a wavelength of 532 nm, produced by a frequency-doubled single-mode Nd:YAG laser. The beam is sent to the resonator via lens L_1, enters the cavity through mirror M_1 (here the beam diameter is ~ 0.5 mm) and excites the Hermite-Gaussian modes of the cavity. The focal length of lens L_1 equals distance A_3, so that the (dotted) beam is injected parallel to the optical axis, independent of the rotation-angle of mirror M_3. This allows us to vary Δr, the off-axis position of injection on mirror M_1, independent of the angle of injection. We inject in the xz-principal plane or in the y-principal plane in order to excite only 1-dimensional TEM_{m0} or TEM_{0m} modes. Exciting a limited set of modes makes labelling of the modes easier and allows us to measure closer to degeneracy. The spectrum is obtained from the spatially integrated throughput as a function of the cavity length, by scanning the position of mirror M_1 with a piezo-element. Judging from these spectra, we estimate the finesse of the cavity as ~ 5600 for low-order modes and ~ 5000 for high-order modes. This is considerably smaller than the value of the finesse allowed by the mirror reflectivities ($> 99.995\%$). We attribute this discrepancy mainly to scattering due to polishing errors of the mirrors.

The length L of the cavity is varied by changing the length of arm A_1; this length is chosen such that the spectrum is almost N-fold degenerate resulting in N "clumps" of modes (see Fig. 5.3). Fig. 5.4 shows a detail of the modes within the "fundamental" clump. The mode number difference of subsequent modes is N. The transverse mode numbers of the modes within this clump are thus labelled $m = lN$, where $l = 0, 1, 2,$ etc.

The closeness to degeneracy is illustrated by the typical distance between subsequent peaks $\Delta\nu_N/\Delta\nu_{\mathrm{FSR}} \approx 1\times10^{-3}$, where $\Delta\nu_N$ is the distance between mode $m = 0$ and mode N and $\Delta\nu_{\mathrm{FSR}}$ is a free spectral range. Higher-order modes are therefore still relatively close to the $m = 0$ mode so that the effect of vibrations on the time scale of the piezo scan is limited (we scan typically over $\Delta\nu_{\mathrm{FSR}}$ in ~ 22 ms). Specifically, for a frequency range $\Delta\nu_{\mathrm{FSR}}/16$ ($m \approx 500$)), the measured vibration-induced fluctuations in $\Delta\nu/\Delta\nu_{\mathrm{FSR}}$ are of the order 3×10^{-4}. This is acceptable as in our range of mode numbers (m up to 1500) the modes can still be labelled uniquely, ($3\times10^{-4} < 1\times10^{-3}$).

To find the Gouy phase as a function of mode number, a set of $15-25$ spectra is measured for increasing off-axis position of injection, Δr. Every time the off-axis distance of the beam is increased, a different clump of peaks containing higher-order Hermite-Gaussian modes is

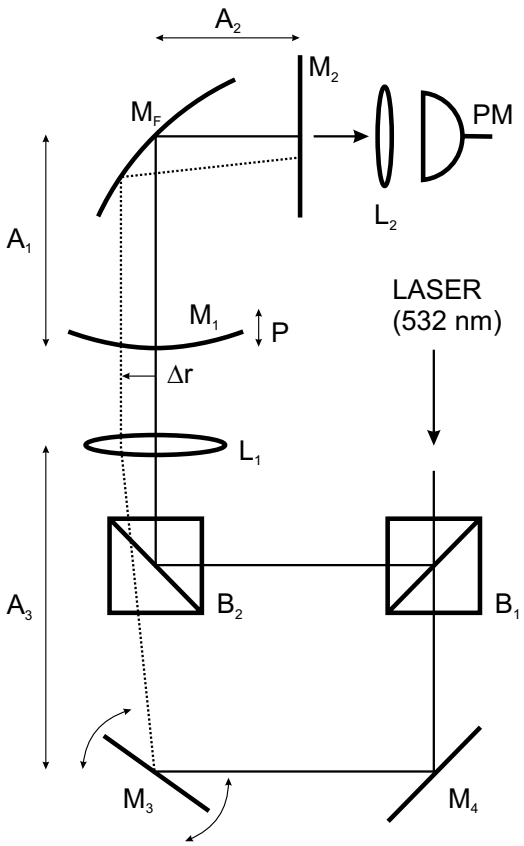

Figure 5.2: *Overview of the setup, where the mirrors M_1, M_F and M_2 form the folded resonator. A_1, A_2: lengths of resonator arms, PM: photomultiplier, L_1, L_2: lenses, B_1, B_2: beamsplitters, M_3, M_4: mirrors. The solid line indicates the fixed beam which excites the fundamental mode. The position of the other (dotted) beam on mirror M_1 can be increased by rotating M_3 to excite higher-order modes.*

excited. Starting from the on-axis position, the position of injection is increased stepwise such that the spectra of successive measurements overlap. Finally, a second beam is always injected into the resonator to excite only the fundamental ($m = 0$) mode. The presence of this reference mode, in the set of overlapping spectra, allows for a unique labelling up to transverse mode numbers $m \approx 1500$.

5.4 Experimental results

For every transverse mode m, the frequency difference $\Delta\nu_m$ is measured and this is transformed to a round-trip Gouy phase by using Eq. 5.4. For several degenerate configurations ($N = 7$, 8, and 9), the change of the Gouy phase as a function of the mode number has thus

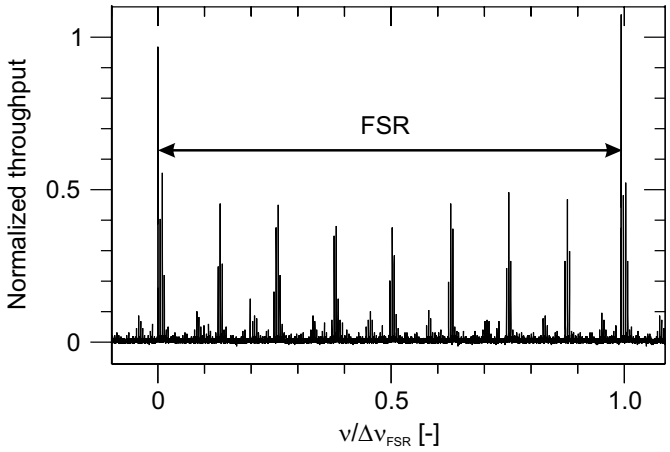

Figure 5.3: *Spectrum for an almost* 8*-fold degenerate cavity configuration. The modes collapse into* 8 *clumps of peaks. The two highest peaks are due to the fundamental mode, which serves as a reference.*

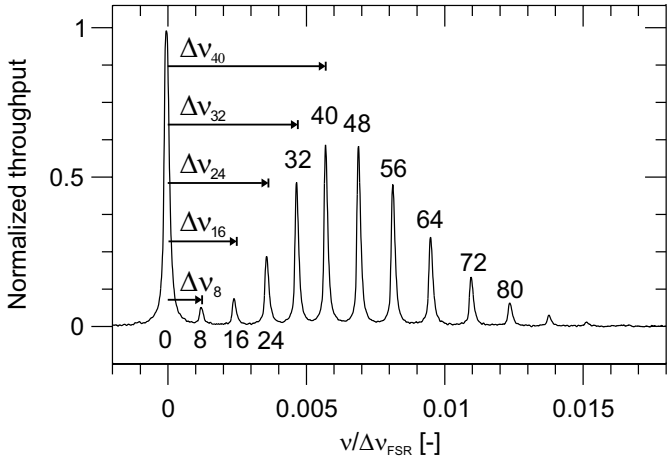

Figure 5.4: *Spectral detail of the fundamental mode and the nearest clump of peaks. The almost 8-fold degeneracy makes the difference in mode number between two subsequent modes equal to 8.* $\Delta\nu_m$ *is the distance between the fundamental mode* $m = 0$ *and mode m.*

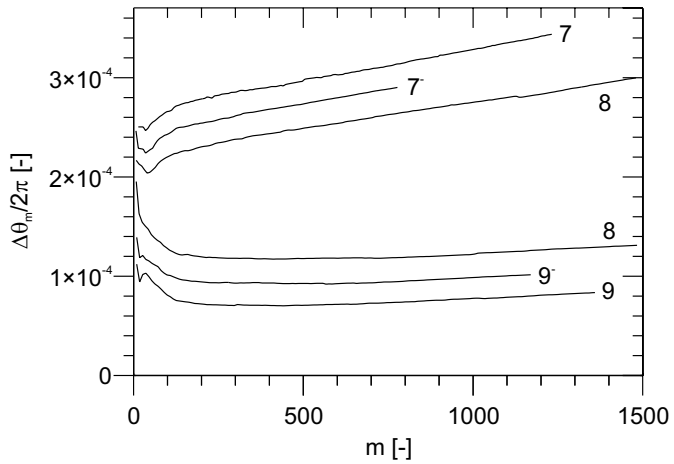

Figure 5.5: *$\Delta\theta_m$ vs. mode number m for various values of N. The upper three curves are measured in the xz-principal plane, the lower ones in the y-principal plane. For easy comparison all curves have been vertically shifted by an arbitrary amount to bring them closer to each other; the N^- indicates an originally negative valued $\Delta\theta_m$.*

been determined. Fig. 5.5 shows the measured value of $\Delta\theta_m/2\pi$ as a function of the transverse mode number m. The three top curves show this dependence for displacements of the injected beam in the xz-principal plane (for orientation see Fig. 5.1), at three different but fixed cavity lengths, corresponding to degeneracy near $N = 7$, somewhat below 7 (denoted 7^-) and near $N = 8$. The three bottom curves show this dependence for displacements in the y-principal plane for $N \simeq 8, 9^-$ and 9. As only the *change* of $\Delta\theta_m$ with m is important, a suitable vertical offset has been added to the various curves to allow better comparison.

The change of $\Delta\theta_m$ with m is a nonparaxial effect that corresponds with the onset of aberrations. For $N = 8$ in the xz-principal plane, $\Delta\theta_m/2\pi$ increases with 0.7×10^{-4} when going from for low m-values to $m \approx 1200$. In this region, $\Delta\theta_m/2\pi$ changes in the y-principal plane with only 0.1×10^{-4}. We thus find almost an order of magnitude stronger aberrations in the xz-principal plane than in the y-principal plane. We attribute this key result to the fact that modes in the y-principal plane will hardly feel the aberrations due to the folding mirror, M_2, in contrast to the modes in the xz-principal plane.

Varying the degree of degeneracy, N changes the position and angle of incidence at which the rays hit the optical elements. On this basis, one could expect that the change of the Gouy phase depends on N. More detailed inspection of Fig. 5.5 shows first of all that the Gouy phase is practically independent of the odd/even nature of the number of hit points, N, on the mirrors. Secondly, $\Delta\theta_m$ shows a strange wiggling for the lower-order mode numbers, $m = 0$ up to 150. A likely explanation for this phenomenon is in the surface polishing errors of the mirrors [56]. These imperfections are expected to affect the lower-order modes much stronger than the higher-order ones, as the latter have larger transverse mode sizes and should thus smooth out local errors in the shape of the mirrors.

In order to enable a comparison of the experiment with ray-tracing simulations (see Sec-

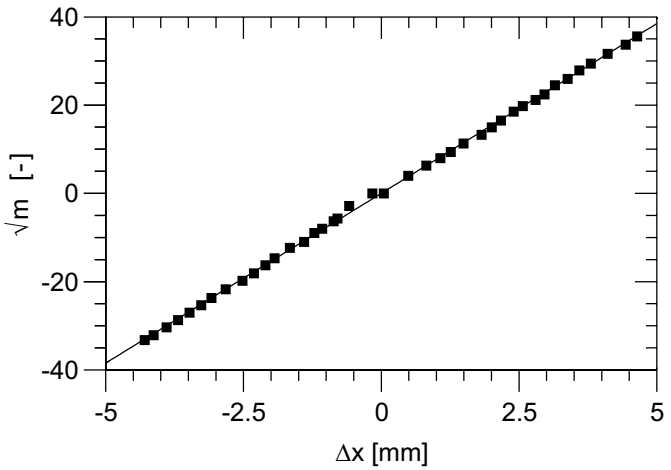

Figure 5.6: *The square root of the mode number vs. the off-axis distance of injection on mirror M_1.*

tion 5.5), we have measured the relation between the dominantly excited mode number and the off-axis injection distance. The experimental result for $N = 8$ is shown in Fig. 5.6, where the negative/positive square roots of the mode numbers refer to injection on the right/left side of the marker mode on mirror M_1. The linear fit was used to determine both the slope and the $\Delta x = 0$ point. Paraxial theory predicts that the mode number changes approximately quadratically with the ratio of the off-axis distance and the waist of the fundamental Gaussian mode w_0: $m \sim (\Delta r/w_0)^2$ [12]. The fitted curve shows that this paraxial dependence is not yet violated in our folded cavity; this is in accordance with the results of Laabs [57] for a two-mirror cavity.

5.5 Comparison with ray tracing

Since the Gouy phase is also a ray-optical property, it can be calculated by means of a ray-tracing program. We did this for a ray that is injected parallel to the optical axis from a certain off-axis distance Δr through the folded resonator, configured close to degeneracy N. The positions of the ray on the first (injection) mirror are calculated exactly for $n = 10^4$ round-trips. As shown in Herriot *et al.* [21] the hit points x_n on the mirror are given by

$$x_n = \Delta r \cos[n\theta(\Delta r)] \,, \tag{5.5}$$

where Δr is the off-axis distance of injection. This allows us to calculate the Gouy phase $\theta(\Delta r)$ from the 10^4 points x_n, with an accuracy of approximately 10^{-6} rad.

The results of calculations for an $N = 8$ and 9 three-mirror cavity are depicted in Fig. 5.7, which displays $\Delta\theta/2\pi$ as a function of the off-axis distance of injection, Δr. The calculations show that the Gouy phase is not a constant but increases with Δr. Furthermore, the Gouy phase changes much stronger for increasing displacements in the xz-principal plane than in the y-principal plane; we compare this now with the experimental results.

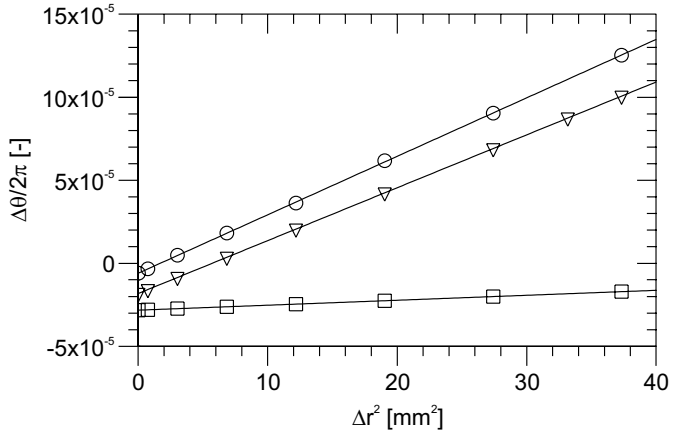

Figure 5.7: *Ray-tracing calculations of $\Delta\theta$ vs. the square of the off-axis distance (xz-principal plane) of injection for $N = 8$ (triangles) and 9 (circles) and in the y-principal plane for $N = 9$ (squares).*

For injection in the xz-principal plane (Δr becomes Δx) the calculated slope $\Delta\theta_m/(\Delta x)^2$ for $N = 8$ is 1.97×10^{-5} rad/mm^2. To compare this to the experiment we take the linear fit of the measured data for $N = 8$ (Fig. 5.5) which is converted from mode number to off-axis distance of injection, using Fig. 5.6. This results in an experimental slope $\Delta\theta_m/(\Delta x)^2 = 2.00 \times 10^{-5}$ rad/mm^2. The excellent agreement between theory and experiment validates our mapping from ray to wave dynamics.

To put these numbers in perspective, we consider the specific case of injection at $\Delta x =$ 5 mm, which excites a group of modes around mode number $m = 1500$. From the slope given above, this produces a (nonparaxial) change of the Gouy phase $\Delta\theta_m$ by $\sim 5 \times 10^{-4}$ rad as compared to the paraxial values θ_0. Although this number is small, it can be measured relatively easily in our system because the shift in resonance frequency of a mode is proportional to $m\Delta\theta_m \approx 0.75$ rad $\approx 0.12\ \Delta\nu_{\mathrm{FSR}}$ in the considered case. This is easily observable in our high-finesse cavity.

For a better understanding of the strength of the aberrations in the folded resonator, we have also studied a two-mirror cavity, both experimentally and theoretically. In this case, we choose two mirror radii of 1 m and a cavity length L of ~ 8 cm, which corresponds to a degeneracy near $N = 8$. Due to the absence of astigmatism, we observed a strong coupling between the horizontal and vertical modes, which made the measurement less accurate. Experimental results show that the change in $\Delta\theta_m/2\pi$ is less than 3×10^{-5} up to $m \approx 1000$. The calculation of the Gouy phase, which, in the present case, is more accurate than its measurement, shows a small increase of the Gouy phase for increasing mode numbers. The slope of the calculated Gouy phase as a function of the off-axis distance on the first mirror is 1.3×10^{-6} rad/mm^2, which is equivalent to $\Delta\theta_m/2\pi = 5 \times 10^{-6}$ for $m \approx 1000$.

5.6 Comparison with aberration theory

In a general optical system with a given object plane, the number of third-order aberrations depends on the symmetry of the system and is at most 20 [58]. For a rotationally symmetric system, like a cavity consisting of two spherical mirrors, the number of independent aberration coefficients is reduced to only 5, also known as the Seidel aberrations, being: spherical aberration, coma, astigmatism, curvature of field and distortion (see a.o., [14]). An aberration can be expressed in two ways: as a deviation from a reference wave front in the exit pupil (wave aberration) or as a displacement from the image point in the image plane (ray aberration). A ray-aberration is the spatial derivative of the corresponding wave-aberration; the wave aberrations are fourth-order and the ray-aberrations are third-order in the spatial coordinates (see a.o. [59]). In the literature, an aberration is usually indicated by the order of the ray-aberration.

The comparison of our experimental results with standard optical aberration theory is hampered by the fact that aberrations in a round-trip cavity, or in the equivalent periodic lens guide, are hardly discussed in the literature. Furthermore, our 3-mirror folded (not to be confused with the terminology "folded/unfolded" in the context of equivalent periodic lens guides [12]) resonator does not fall in the usual category of rotational symmetric systems, for which the standard Seidel aberrations apply. In this largely unchartered territory, we will rely on some general arguments, which are necessarily of a qualitative nature.

To link the observed nonparaxial behavior with aberration theory, we consider the two principal planes of the equivalent lensguide, one that is orthogonal to the folded axis (Fig. 5.8a) and one that contains the folded axis (Fig. 5.8b). In the former case (y-principal plane), the mirror symmetry, demonstrated in Fig. 5.8a, makes that the lowest nonvanishing aberrations are the usual third-order aberrations. In fact, we find the magnitude of the aberrations in the y-principal plane of the folded resonator to be of the same order for the folded resonator as for a regular two-mirror resonator. However, this symmetry is absent in the xz-principal plane. Fig. 5.8b shows how the folding mirror can be represented in corresponding lens guide by alternating forward- and backward-tilted lenses. The aberrations in the xz-principal plane are therefore potentially much stronger as they also contain second-order terms [60, 61].

However, due to the *periodic* nature of our (round-trip) optical system, one can show, that these second-order terms average out. To perform this averaging, we should add the aberrations over consecutive round-trips, preferably by expressing them in special "scaled variables" that are invariant under paraxial propagation [14]. For ray-aberrations, this rewrite comprises a multiplication with oscillating terms of the form $\cos(n\theta)$ and $\sin(n\theta)$ (see Eq. 5.5). This leads to the mentioned cancellation of second-order (ray-)aberrations. From the perspective of wave-aberrations, we have to add simply the folding-induced aberrations in the optical wavefront. As the associated wave aberrations are third-order in the ray coordinates and as these coordinates oscillate periodically, the odd-order wave aberrations are just as often positive as negative and will cancel as well. This leads us to the surprising conclusion that also in the xz-principal plane we are left with the usual third-order (Seidel) aberrations. The magnitude of these terms is observed to be about a factor 10 larger than in the y-principal plane (*cf.* Fig. 5.7). This increased magnitude results from the lenses being tilted in the xz-principal plane and is apparently caused by the off-axis aberrations of the individual lenses in Fig. 5.8b.

The observed linear dependence of Gouy phase on mode number, in the form $\theta_m \simeq a +$

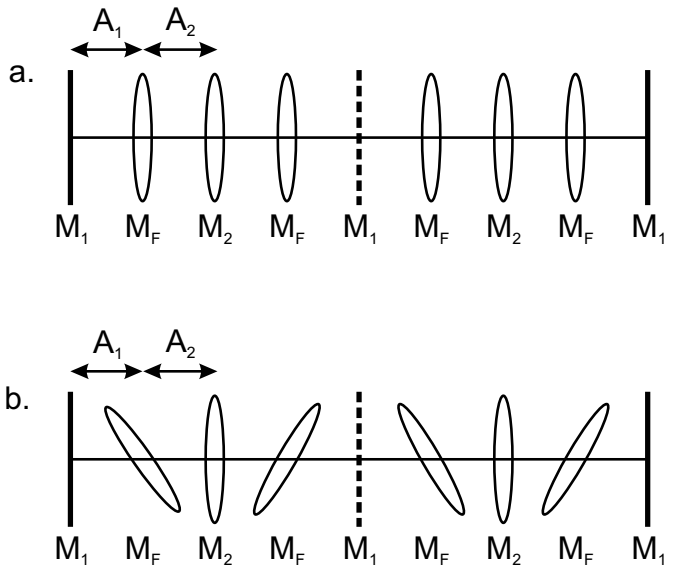

Figure 5.8: *The equivalent lens guide of a folded 3-mirror resonator in the xz-principal plane and the y-principal plane for two round-trips.*

bm, is consistent with this effectively third-order of the ray aberrations. To appreciate this statement, one should realize that the phase acquired by a transverse mode m (in comparison to mode $m = 0$) is $m\theta_m$, and that m depends quadratically on the off-axis distance Δr. This means that the nonparaxial term bm corresponds to a phase change that scales with the fourth power of Δr. Fourth-order changes in path length of the wave aberrations correspond to the Seidel aberrations.

The magnitude of the *individual* Seidel-aberrations of the lens guide in Fig. 5.8 can not be derived from our measurements or calculations. Only the *sum* of all Seidel coefficients is obtained, as they all exhibit the same scaling with ray coordinates after repetitive passage through the cavity. The magnitude of the unit of the aberrations is expressed as the phase shift divided by the off-axis distance of injection squared, being, *e.g.*, 2×10^{-5} rad/mm^2 for $N = 8$. We note that the observed increase in Gouy phase with the fourth-order off-axis distance is consistent with the sign and scaling found by Hercher [19].

5.7 Conclusions

We have demonstrated a very accurate method to measure the Gouy phase as a function of the mode number. For the folded three-mirror cavity, we found that the Gouy phase for the modes in the *xz*-principal plane changes is much stronger than its y-plane counterpart. A connection between the Gouy phase and aberration theory has been established. Effectively, the aberrations of a folded resonator behave as the Seidel aberrations, in spite of the lack of rotational symmetry. These results are supported by ray-tracing calculations; all calculations

are in very good agreement with the measurements.

5.8 Acknowledgement

We thank prof. J. J. M. Braat for discussions and dr. A. Aiello for the use of his ray-tracing software.